Modified Auxiliary-Resonant Commutated Pole Applied in a Three-Phase Dual-Active Bridge DC/DC Converter

Johannes Voss and Rik W. De Doncker

***Abstract*—The purpose of this study is to present the concept and properties of a dual-active bridge dc–dc converter with a modified auxiliary-resonant commutated (MARC) pole concept, and to discuss preliminary test results of a high-power setup. In this approach, the dual-active bridge based on IGCT is considered. First, the soft-switching boundaries for the converter with lossless snubbers and high switching delays are introduced. Second, the MARC pole is presented to overcome this border to receive full soft-switching capability in the entire operation range of the dc–dc converter. This is of crucial importance since IGCTs will be destroyed in case of a snubber dump. The advantage of the modified circuit is the guaranteed switching under zero-voltage conditions without applying an additional boost current as needed in the classic auxiliary-resonant commutated pole (ARCP) approach. Thus, complexity is reduced and reliability is increased. Measurement results of the MARC are presented from a mega-watt dc–dc converter where the concepts are fully implemented. The results of large-scale systems impressively show how the ARCP reduced the impact of parasitic elements, which would normally affect the switching transitions tremendously.**

***Index Terms*—DC-DC power converters, zero-voltage switching, three-phase electric power, snubbers.**

I. Motivation

TODAY's renewable energy sector is growing steadily. Renewable power plants in the MW range, such as wind turbines, are primarily connected to the medium-voltage level [1]. In contrast to wind turbines, for example, photovoltaic cells which are installed on private roof tops are connected at low-voltage levels. Both systems feed power back into different voltage levels. Thus, the classic top-down structure of distribution grids, where the high-voltage grid classically feeds the lower voltage levels, changes towards a structure, which allows bidirectional power flow. In terms of controlling this power flow, direct current (dc) grids with power electronic converters have advantages over classic alternating current (ac) solutions with forced commutating behavior [2]. Therefore, a connection equivalent to a 50 Hz transformer in ac systems is needed between different dc voltage levels. A dc–dc converter suitable for this application is the dual-active bridge (DAB) converter [3]–[6], as shown in Fig. 1. This converter allows a bidirectional power flow and ensures galvanic isolation. Due to its wide soft-switching range, it reaches high efficiencies and is compatible with 50 Hz transformers. Such a dc–dc converter has been built at the E.ON Energy Research Center based on integrated gate-commutated thyristor (IGCT) Power Electronic Building Blocks (PEBBs). The dc–dc converter will be linked to a 5 kV medium-voltage dc (MVDC) grid, which will connect several test benches that are located at RWTH Aachen University campus. To maximize the efficiency of high-load operations, lossless snubbers are connected to the main switches. However, it is well known that this will limit the soft-switching boundary of the DAB [7].

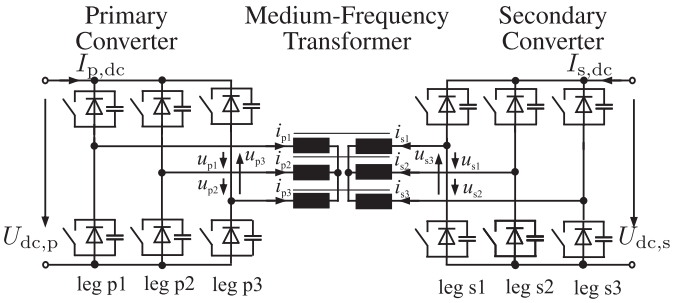

Fig. 1. Two-level dual-active bridge with snubber capacitors.

II. State-of-the-Art

One method to fully ensure soft-switching is the auxiliary-resonant commutated pole (ARCP) first proposed in [8]. It has been shown in literature that the ARCP can reduce the occurring switching losses by almost a factor of eight [9]–[11]. Conventional converters using IGCTs need RCD clamping circuits [12] and di/dt limiters to restrict their operation to the safe operation area (SOA) of the devices. These conventional d$i/$dt limiters must be rated for the total dc-link current and therefore often require water cooling. In part load conditions or at high non-symmetrical input or output voltages, the DAB converter loses its soft-switching capability because the residual magnetic energy stored within the load is insufficient to fully commutate and charge the voltage of the snubber capacitors that are

Manuscript received September 20, 2018; revised December 4, 2018, January 22, 2019, and April 20, 2019; accepted May 15, 2019. Date of publication May 19, 2019; date of current version November 12, 2019. This work is part of the research conducted in the Flexible Electrical Networks Research Campus, Project 2: Equipment and Network Technologies for Medium-Voltage DC Applications, funded by the German Federal Ministry of Education and Research (03SF0489). Recommended for publication by Associate Editor T. Mishima. *(Corresponding author: Johannes Voss.)*

The authors are with the Institute for Power Generation and Storage Systems, RWTH Aachen University 52062, Aachen, Germany (e-mail: post_pgs@eonerc.rwth-aachen.de; dedoncker@ieee.org).

Color versions of one or more of the figures in this paper are available online at http://ieeexplore.ieee.org.

Digital Object Identifier 10.1109/TPEL.2019.2918009

placed across the main power switches. In this work, to ensure soft-switching capability and to avoid the losses of the clamping circuit, a quasi-resonant [13] modified auxiliary-resonant commutated pole (MARC) is applied, as explained in more detail in Section IV. Thus, conventional clamping and snubber systems of an IGCT-based converter are not necessary. The MARC concept, first introduced in [14], proposes two auxiliary inductors, which are rated only for the rms current of the resonant phase and are considerably less expensive than the $\mathrm{d}i/\mathrm{d}t$ limiter in the conventional clamping circuit. In [14], low power tests at 60 V were conducted. In [15], a similar approach for three-level stacks is introduced and experiments were conducted with a dc-link voltage up to 200 V, based on IGBTs for a single converter leg. Another approach for three-level converter leg based on IGBT is introduced in [16]. Here the auxiliary path is magnetized by the full dc-link voltage. Results using a half-bridge are examined at 1200 V. In [17], the auxiliary inductors are replaced by a transformer. This topology only guarantees zero-voltage switching for the lower switches. Instead of forcing a zero-voltage condition per converter leg, e.g., in [18], the dc-link voltage is actively forced into resonance. In [19], another topology for the auxiliary resonant commuted pole is presented to minimize the losses in the auxiliary switches. Example of pulse width modulated converters with ARCP can be found in [20] and [21]. Besides the aim of reducing losses or limiting the $\mathrm{d}u/\mathrm{d}t$, the auxiliary resonant commutated pole is today investigated for EMI reduction with special focus on new semiconductor materials such as SiC or GAN. For example, in [22], benefits in the MHz range were observed. Also, in [23], the ARCP employed EMI reduction without significant efficiency improvements. Other techniques to reach zero-voltage switching without quasi-resonant topologies can be found in [25] or [30]. However, in these approaches, the full operation area is not covered.

III. Soft-Switching Boundaries of a Snubbered DAB Considering High-Switching Delays

In this section, the soft-switching boundaries are summarized and extended, in particularly for high-power devices with high switching delays, which affect the soft-switching boundaries.

The converter topology with snubber capacitor but without ARCP/MARC is given in (1). It consists of two three-phase half-bridges, which are linked by a three-phase transformer. The basic operation mode of the converter is the six-step mode in which the bridges are operated at a duty cycle of 50%. The legs of each converter are shifted in phase by 120° from each other. The transmitted power is set by variation of the phase shift between the primary and secondary phase voltages, known as the load angle φ. This phase shift creates a voltage drop across the transformer leakage inductance, resulting in a power flow between primary and secondary sides.

For the conventional dual-active bridge without snubber capacitors, the soft-switching boundaries can be solved whenever the current crosses zero. In [3], [28], the dynamic voltage ratio $d = U_{\mathrm{dc,s}}/U_{\mathrm{dc,p}}$ is introduced representing the ratio between the primary dc-link voltage and secondary dc-link voltage. The phase shift φ represents the phase-shift between the primary and secondary sides of the six-step voltage as shown in Fig. 2.

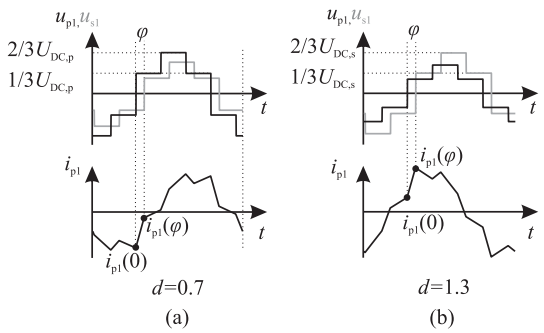

Fig. 2. Basic phase current wave forms of 3PH DAB for (a) $d = 0.7$ and (b) $d = 1.3$.

For example, in Fig. 2, the primary converter bridge for a dynamic voltage ratio of $d = 0.7$ is operating in soft-switching, since the phase current is conducting via the anti-parallel diode and thus the device will turn on at zero voltage. On the other hand, the secondary converter is hard-switched since the current is positive with respect to the secondary side [29]. For $d = 1.3$, the primary converter is hard-switched and the secondary converter is soft-switched, respectively.

The currents in the switching instant for the primary side $i_{\mathrm{p1}}(0)$ and the secondary side $i_{\mathrm{p1}}(\varphi)$ are given in (1) and (2), respectively. To derive the soft-switching boundary, the dynamic voltage ratio $d_{\mathrm{zv}}(\varphi)$ at zero-voltage switching is introduced. Using (1) with $i_{\mathrm{p1}}(0) = 0$ for the primary converter and (2) with $i_{\mathrm{p1}}(\varphi) = 0$ for the secondary bridge results in $d_{\mathrm{zv}}(\varphi)$, which can be found in [30].

The primary-side current at the primary-side switching instant $t = 0$ is

$$i_{\mathrm{p1}}(0) = \frac{U_{\mathrm{dc,p}}}{3X_{\mathrm{ser}}} \cdot \begin{cases} \frac{2\pi d}{3} - d\varphi - \frac{2\pi}{3} & \text{for } 0 \le \varphi \le \frac{\pi}{3} \\ \pi d_{\mathrm{zv}} - 2d\varphi - \frac{2\pi}{3} & \text{for } \frac{\pi}{3} \le \varphi \le \frac{\pi}{2} \end{cases} \tag{1}$$

and the primary-side current at the secondary-side switching instant $t = \varphi$ is

$$i_{\mathrm{p1}}(\varphi) = 0 = \frac{U_{\mathrm{dc,p}}}{3X_{\mathrm{ser}}} \cdot \begin{cases} \varphi + \frac{2\pi d}{3} - \frac{2\pi}{3} & \text{for } 0 \le \varphi \le \frac{\pi}{3} \\ 2\varphi + \frac{2\pi d}{3} - \pi & \text{for } \frac{\pi}{3} \le \varphi \le \frac{\pi}{2} \end{cases} \tag{2}$$

with $X_{\mathrm{ser}} = 2\pi f_{\mathrm{sw}} L_\sigma$

f_{sw} the switching frequency of the converter

L_σ the equivalent inductance of the load.

In (3), the normalized power $p_{\mathrm{norm}}(\varphi)$ excluding the dynamic voltage ratio d is

$$p_{\mathrm{norm}}(\varphi) = \frac{P(\varphi)}{d} \cdot = \frac{U_{\mathrm{dc,p}}^2}{X_{\mathrm{ser}}} \begin{cases} \frac{2\varphi}{3} - \frac{\varphi^2}{2\pi} & \text{for } 0 \le \varphi \le \frac{\pi}{3} \\ \varphi - \frac{\varphi^2}{\pi} - \frac{\pi}{18} & \text{for } \frac{\pi}{3} \le \varphi \le \frac{2\pi}{3} \end{cases} \tag{3}$$

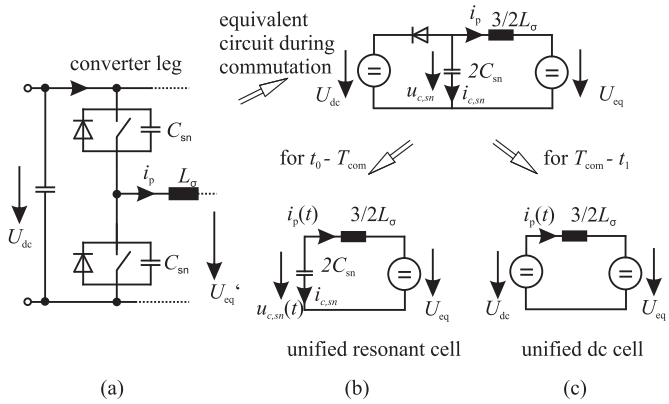

Fig. 3. Unified commutation cell of the dual-active bridge: (a) the converter leg, (b) the unified resonant cell, (c) dc-cell after commutation.

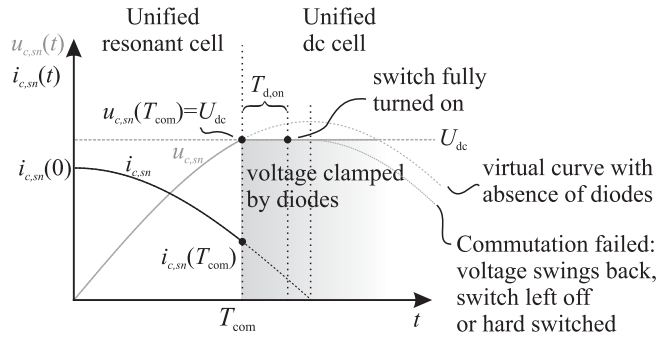

Fig. 4. Resonant commutation including the turn on delays $T_{\mathrm{d,on}}$ of a switch.

The soft-switching boundaries for the primary $P_{\mathrm{zv,p}}(\varphi)$ and for the secondary $P_{\mathrm{zv,s}}(\varphi)$ can then be computed for the primary and secondary converters, as widely explained in the literature [3], [5], [7].

To derive the power at zero-voltage switching for the primary and secondary bridges, the normalized power p_{norm} is multiplied by the dynamic voltage ratio appearing at the soft-switching border (4)

$$\begin{aligned} P_{\mathrm{zv,p}}(\varphi) &= d_{\mathrm{zv,p}}(\varphi) p_{\mathrm{norm}}(\varphi) \\ P_{\mathrm{zv,s}}(\varphi) &= d_{\mathrm{zv,s}}(\varphi) p_{\mathrm{norm}}(\varphi). \end{aligned} \tag{4}$$

In order to increase the efficiency of the converter, lossless snubber capacitors C_{sn} are connected in parallel to the main switching devices as illustrated in Fig. 3. When introducing lossless snubber capacitors, the zero-voltage switching range will be further reduced.

Reactive power is needed to discharge and charge the capacitors, respectively, before switching on the main devices. To reach soft-switching, the phase current has to be of proper direction at the switching instant but should also have sufficient magnitude to commutate the snubber capacitors.

In fact, the circuit of the DAB with snubber capacitors can be reduced to the equivalent resonant pole converter leg as shown in 3(a) [7]. The unified cells represent the transformer leakage inductances multiplied with a factor of 3/2 because the leakage inductances are connected in star. Hence, in the DAB, one is always connected in series with two in parallel. The cell in Fig. 3(b) represents the commutation cell when the capacitors $2C_{\mathrm{sn}}$ are charged.

The reflected equivalent voltage U_{eq} (5) depends on the phase shift φ of the converter and the dynamic voltage ratio d [7].

$$U_{\mathrm{eq}} = \frac{1}{2} \begin{cases} U_{\mathrm{dc,p}}(1+2d) & \text{for } -\frac{\pi}{3} \le \varphi \le -\frac{\pi}{3} \\ U_{\mathrm{dc,p}}(1+d) & \text{for } -\frac{\pi}{3} \le \varphi \le 0 \\ U_{\mathrm{dc,p}}(1-d) & \text{for } 0 \le \varphi \le \frac{\pi}{3} \\ U_{\mathrm{dc,p}}(1-2d) & \text{for } \frac{\pi}{3} \le \varphi \le \frac{\pi}{3}. \end{cases} \tag{5}$$

While for positive phase shifts the reflected equivalent U_{eq} is negative, meaning that the primary side is leading, it is positive for negative phase shifts. In consequence, a lagging phase will always be supported in its commutation process by the other converter leg.

The inductor forces a current into the capacitor $i_{\mathrm{C,sn}}(t)$ and the snubber voltage $u_{\mathrm{C,sn}}(t)$ will rise until it reaches the value of the dc-link voltage U_{DC} within the commutation time T_{com}. This is only true if the energy stored in the inductive elements is high enough to fully commutate the snubber capacitors. When the capacitor voltage reaches U_{DC}, the anti-parallel diode clamps the voltage and the remaining inductive energy is fed back into the dc-link. Therefore, the unified dc commutation cell, as shown in Fig. 3(c), is valid during this sequence. When the diode clamps the current, the main switch is at zero voltage and has to be turned on.

To avoid a snubber dump in the main IGCT switches, the gate signals $\mathrm{G_{MAIN}}$ must be released first by a high-speed zero-voltage detection (ZVD) [33]. Here, the turn-on delay of the gate drivers and the switches (3.5 µs [40], [35]) as well as the ZVD time (1.5 µs [33]) is summarized in $T_{\mathrm{d,on}}$. If the current is not high enough to overcome the delay $T_{\mathrm{d,on}}$, the capacitor voltage swings back, and soft-switching would fail. This may result in an unwanted hard-switching event (snubber dump) with the potential to destroy the switch, unless the switch will be left off, which would halt the DAB operation. In Fig. 4, a resonant commutation is sketched.

The analytical solution (6) for the capacitor voltage $u_{\mathrm{C,sn}}(t)$ and the phase current $i_{\mathrm{p}}(t)$ during the resonant commutation is described by

$$\begin{aligned} u_{\mathrm{C,sn}}(t) &= i_{\mathrm{p}}(0) Z_{\mathrm{r}} \sin(w_{\mathrm{r}} t) - U_{\mathrm{eq}} \cos(w_{\mathrm{r}} t) + U_{\mathrm{eq}} \\ -i_{\mathrm{p}}(t) &= i_{\mathrm{p}}(0) \cos(w_{\mathrm{r}} t) - \frac{U_{\mathrm{eq}}}{Z_{\mathrm{r}}} \sin(w_{\mathrm{r}} t) \\ \text{with } Z_{\mathrm{r}} &= \sqrt{\frac{3L_\sigma}{4C_{\mathrm{sn}}}} \text{ and } w_{\mathrm{r}} = \frac{1}{\sqrt{3L_\sigma C_{\mathrm{sn}}}} \end{aligned} \tag{6}$$

with the current $i_{\mathrm{p}}(0)$ at the switching instant of the primary side (1). Due to symmetry, only the primary converter is considered here.

Using the values given in Table I, the commutation times at three operation points according to the introduced equations are plotted in Fig. 5.

TABLE I
CHARACTERISTICS OF THE CONVERTER

	Value
$U_{\mathrm{dc,nom}}$	5 kV
d	0.8...1.2
f_{sw}	1 kHz
L_σ	185 µH
C_{sn}	0.68 µF
$T_{\mathrm{d,on}}$	1.5 µs + 3.5 µs

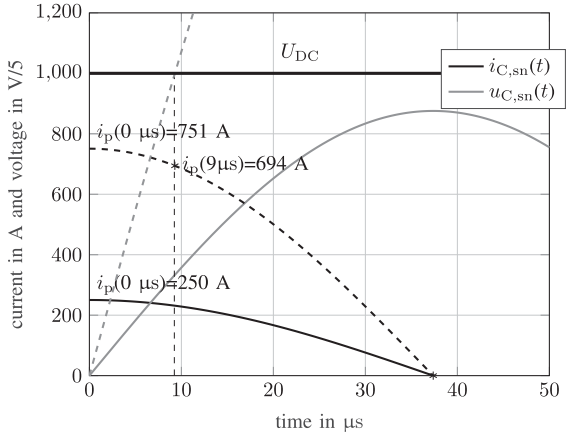

Fig. 5. Transient behavior of the resonant cell for $d = 1$, $C_{\mathrm{sn}} = 0.68$ µF at various load angles $\varphi = 15°, 45°$.

A load angle of $\varphi = 45°$ corresponds to a switching current of $i_{\mathrm{p}}(0) = 751$ A. In this case, the commutation time T_{com} is 9 µs and the remaining current is about 674 A high. In case $\varphi = 15°$, the current at the switching instant is $i_{\mathrm{p}}(0) = 250$ A and a non-successful commutation occurs. The phase current falls to zero and the voltage of the switch does not reach the dc-link voltage.

Similar effects are observed when the size of the resonant capacitor is changed from $C_{\mathrm{sn}} = 0.25$ to 1.5 µF as shown in Fig. 6. At a load angle of $\varphi = 30°$, a phase current of 501 A in the switching instant is present. The commutation time T_{com} tremendously increases from 5 µs up to 27 µs.

The plot illustrates that due to the relatively low leakage inductance L_σ of the DAB transformer, a constant load current cannot be considered. This is often done for motor drives or grid-connected active rectifiers with very large inductors.

Additionally, the phase current does not only have to be high enough to commutate the snubbers, but also high enough to allow a sufficient diode clamping time to overcome the turn on delay $T_{\mathrm{d,on}}$ of the main power switches (7)

$$i_{\mathrm{p}}(T_{\mathrm{com}})_{T_{\mathrm{d,on}}} \geq \frac{2T_{\mathrm{d,on}}}{3L_\sigma}(U_{\mathrm{DC}} - U_{\mathrm{eq}}). \tag{7}$$

In the following, the current at T_{com}, which is high enough to fulfill minimal required diode conduction time, is named $i_{\mathrm{p}}(T_{\mathrm{com}})_{T_{\mathrm{d,on}}}$. To derive the dynamic voltage ratios $d_{\mathrm{zv,Td,p}}$ and

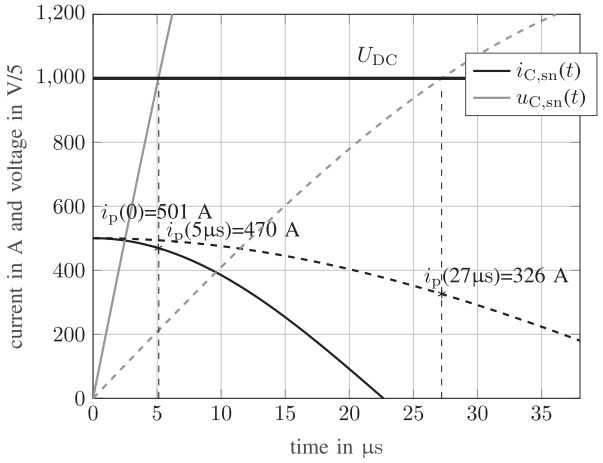

Fig. 6. Transient behavior of the resonant cell for $d = 1, \varphi = 30°$ with various snubber capacitors $C_{\mathrm{sn}} = 0.25$ µF, 1.5 µF.

$d_{\mathrm{zv,Td,s}}$ for the converter with snubbers and switching delays, the energy balance is considered (8)

$$\begin{aligned} \Delta E_{\mathrm{i,p}} &\geq E_{\mathrm{C,SN}} \\ \frac{3}{2}L_\sigma\left(i_{\mathrm{p}}(0)^2_{T_{\mathrm{d,on}}} - i_{\mathrm{p}}(T_{\mathrm{com}})^2_{T_{\mathrm{d,on}}}\right) &\geq C_{\mathrm{sn}}U^2_{\mathrm{DC}} \\ \frac{3}{2}L_\sigma\left(i_{\mathrm{p}}(\varphi)^2_{T_{\mathrm{d,on}}} - i_{\mathrm{p}}(T_{\mathrm{com}})^2_{T_{\mathrm{d,on}}}\right) &\geq C_{\mathrm{sn}}U^2_{\mathrm{DC}}. \end{aligned} \tag{8}$$

The equation introduces the energy in the inductive elements of the transformer $\Delta E_{\mathrm{i,p}}$, which must be as high as the energy $E_{\mathrm{C,SN}}$ to fully commutate the snubber capacitors. The residual energy stored in the inductive elements has to ensure a demagnetization over $T_{\mathrm{d,on}}$.

Using (1), (2) and (8), (9), the dynamic voltage ratios $d_{\mathrm{zv,Td,p}}(\varphi)$ and $d_{\mathrm{zv,Td,s}}(\varphi)$ can be derived, as given in (12). Since the converter is not operating in the SOA for $\varphi > \frac{\pi}{3}$ (phase currents exceeds the rms transformer currents), calculations in this area are ignored.

The current in the switching instant $i_{\mathrm{p1}}(0)$ must be as high as the derived current with the unified resonant cell $i_{\mathrm{p}}(0)_{T_{\mathrm{d,on}}}$

$$\begin{aligned} i_{\mathrm{p}}(0)_{T_{\mathrm{d,on}}} &= i_{\mathrm{p1}}(0) \\ i_{\mathrm{p}}(\varphi)_{T_{\mathrm{d,on}}} &= i_{\mathrm{p1}}(\varphi) \end{aligned} \tag{9}$$

The commutation time T_{com} can then be given as (10) shown at the bottom of this page, and also the load angle for the primary and secondary sides where both conditions given in (9) are fulfilled

$$\begin{aligned} \varphi_{\mathrm{zv,T_{d,on},p}} &= \frac{1}{3d}\Big(3w\sqrt{12C_{\mathrm{sn}}L_\sigma + (d+1)^2T^2_{\mathrm{d,on}}} \\ &\quad +2\pi d - 2\pi\Big) \\ \varphi_{\mathrm{zv,T_{d,on},s}} &= w\sqrt{12C_{\mathrm{sn}}L_\sigma + (d+1)^2T^2_{\mathrm{d,on}}} - 2/3\pi(d-1). \end{aligned} \tag{11}$$

$$T_{\mathrm{com}} = \tfrac{1}{w_{\mathrm{r}}}\arccos\left(\frac{\sqrt{3L_\sigma i_{\mathrm{p}}(0)^2(-4C_{\mathrm{sn}}U^2_{\mathrm{dc,p}}+8C_{\mathrm{sn}}U_{\mathrm{dc,p}}U_{\mathrm{eq}}+3i_{\mathrm{p}}(0)^2L_\sigma)}-4C_{\mathrm{sn}}U_{\mathrm{dc,p}}U_{\mathrm{eq}}+4C_{\mathrm{sn}}U^2_{\mathrm{eq}}}{4C_{\mathrm{sn}}U^2_{\mathrm{eq}}+3i^2_{\mathrm{p}}L_\sigma}\right) \tag{10}$$

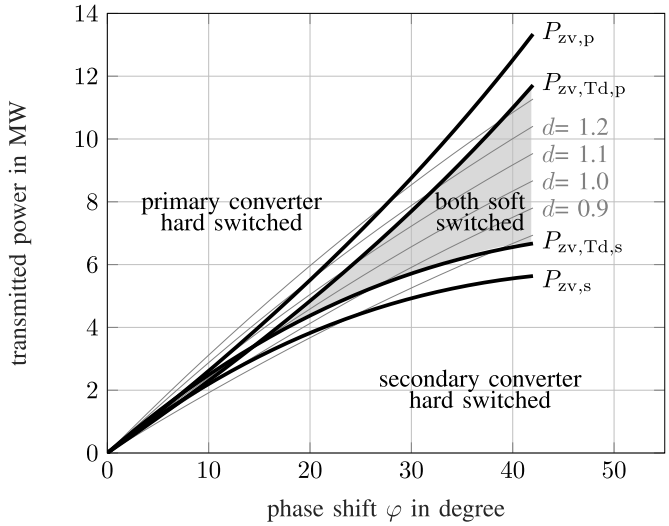

Fig. 7. Soft-switching boundaries of DAB without snubbers ($P_{\mathrm{zv,p}}$, $P_{\mathrm{zv,s}}$) and boundaries ($P_{\mathrm{zv,Td,p}}$,$P_{\mathrm{zv,Td,s}}$) of DAB with snubbers and delays with $C_{\mathrm{sn}} = 0.68$ µF and turn-on delay of $T_{\mathrm{d,on}} = 5$ µs.

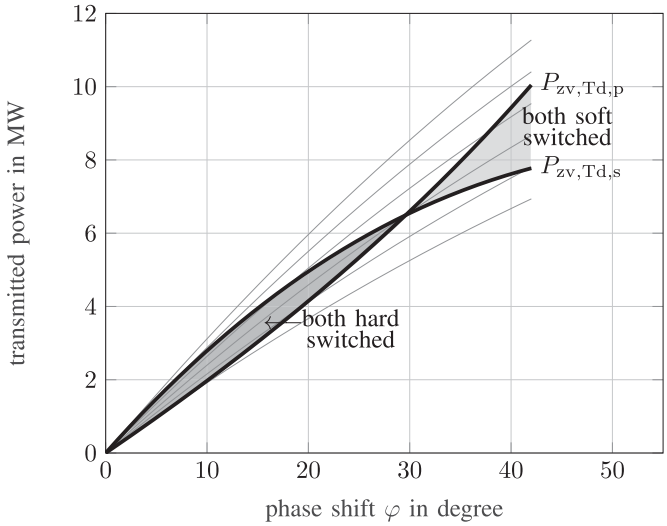

Fig. 8. Soft-switching boundaries ($P_{\mathrm{zv,Td,p}}$,$P_{\mathrm{zv,Td,s}}$) of the extended converter with $C_{\mathrm{sn}} = 3$ µF and $T_{\mathrm{d,on}} = 5$ µs. The converter only reaches soft-switching at higher phase shifts, $\varphi > 30°$.

Solving (11) for the dynamic voltage ratios $d_{\mathrm{zv,Td,p}}$ and $d_{\mathrm{zv,Td,s}}$ leads to (12) shown at the bottom of this page.

The power $P_{\mathrm{zv,Td,p}}$ describes the soft-switching boundaries of the converter extended with snubber capacitors and switching delays according to (13). Fig. 7 illustrates the difference of the the conventional converter without snubbers and ideal switching behavior versus a converter with snubbers and switching delays.

By use of $d_{\mathrm{zv,Td,p}}$ and $d_{\mathrm{zv,Td,s}}$ the transmitted power for soft-switching can be calculated as

$$\begin{aligned} P_{\mathrm{zv,Td,p}}(\varphi) &= d_{\mathrm{zv,Td,p}}(\varphi) p_{\mathrm{norm}}(\varphi) \\ P_{\mathrm{zv,Td,s}}(\varphi) &= d_{\mathrm{zv,Td,s}}(\varphi) p_{\mathrm{norm}}(\varphi). \end{aligned} \tag{13}$$

When introducing snubbers or considering switching delays, even for $d = 1$, the DAB converter is hard-switched in a wide operation range, as illustrated in Fig. 8 with $C_{\mathrm{sn}} = 3\,\mu\mathrm{F}$ and $T_{\mathrm{d,on}} = 5\,\mu\mathrm{s}$.

In Fig. 9, the minimal required phase current to ensure soft-switching at the switching instant is plotted using (1), (2), and (11). For $d = 1$, a symmetrical operation is given and thus the same minimal currents for the primary and secondary appear. Hence, for $C_{\mathrm{sn}} = 0.68\,\mu\mathrm{F}$ and $T_{\mathrm{d,on}} = 5\,\mu\mathrm{s}$, the phase current in the switching instant must fulfill $|i_{\mathrm{p}}| \gtrsim 361A$ for $d = 1$.

To overcome the limited soft-switching area due to the minimal current restriction of a snubbered IGCT-based DAB converter without violating the di/dt restrictions for IGCTs, the modified ARCP will be introduced in the following section.

IV. Introduction of the Modified-Auxiliary Resonant Commutated (MARC) Pole

As mentioned previously, the ARCP is widely discussed in the literature. The general sequences of the modified auxiliary resonant commutated MARC pole are very similar to the classic ARCP and thus only the main differences are introduced. To design the size of the resonant elements, we refer to [10], [31], and [11]. Various boost current strategies have been introduced in [32] and [33]. Also, a special optimized GCT driver for soft-switching operation has been proposed in [34]. The MARC concept will help to overcome some challenges of the ARCP converters such as accurate boost current control [32].

In the following, "classical ARCP" refers to an ARCP phase leg with auxiliary resonant inductors connected to the dc midpoint voltage. The MARC [14], [26], and [27] is based on a separated dc-link with three parts as shown in Fig. 10. The natural behavior of an LC resonant tank is to oscillate to twice the dc voltage behind the inductor. Hence, in the classic lossless ARCP

$$d_{\mathrm{zv,Td,p}} = \frac{-\sqrt{(12\pi\varphi - 18T_{\mathrm{d,on}}^2 w^2 - 8\pi^2)^2 - 4(9\varphi^2 - 12\pi\varphi - 9T_{\mathrm{d,on}}^2 w^2 + 4\pi^2)(-108C_{\mathrm{sn}}L_\sigma w^2 - 9T_{\mathrm{d,on}}^2 w^2 + 4\pi^2)} - 12\pi\varphi + 18T_{\mathrm{d,on}}^2 w^2 + 8\pi^2}{2(9\varphi^2 - 12\pi\varphi - 9T_{\mathrm{d,on}}^2 w^2 + 4pi^2)}$$

$$d_{\mathrm{zv,Td,s}} = \frac{-3\sqrt{-108C_{\mathrm{sn}}L_{\mathrm{aux}}T_{\mathrm{d,on}}^2 w^4 + 48\pi^2 C_{\mathrm{sn}}L_{\mathrm{aux}}w^2 + 9\varphi^2 T_{\mathrm{d,on}}^2 w^2 - 24\pi\varphi T_{\mathrm{d,on}}^2 w^2 + 16\pi^2 T_{\mathrm{d,on}}^2 w^2} + 6\pi\varphi - 9T_{\mathrm{d,on}}^2 w^2 - 4\pi^2}{9T_{\mathrm{d,on}}^2 w^2 - 4\pi^2} \tag{12}$$

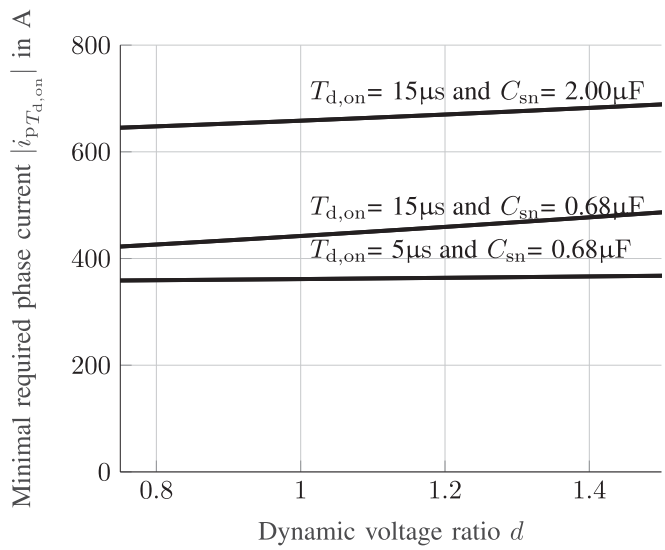

Fig. 9. Minimal phase current to ensure zero-voltage switching.

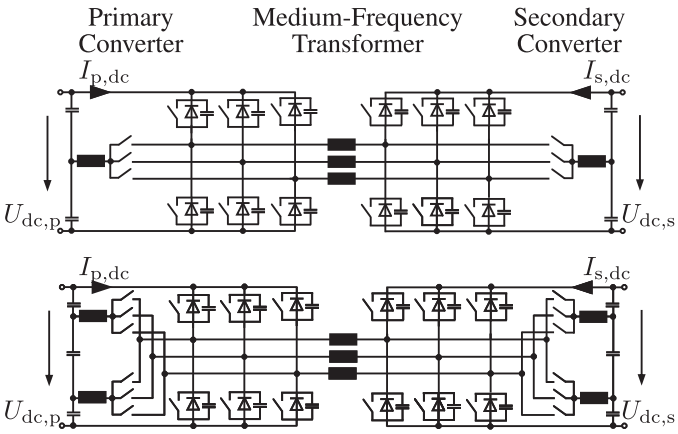

Fig. 10. Simplified circuits of a three-phase DAB with classic auxiliary-resonant commutated pole (top) and the modified auxiliary-resonant commutated (MARC) pole extension.

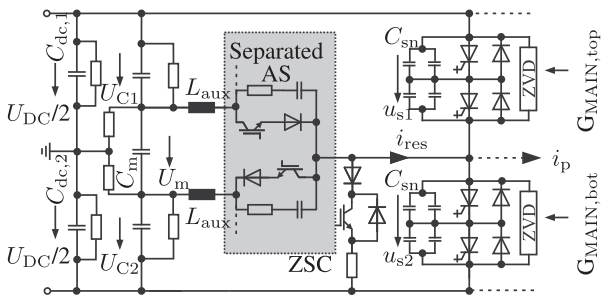

Fig. 11. MARC topology of one leg in detail with separated auxiliary switches (AS), balancing resistors, zero-voltage detection (ZVD), and zero-state chopper (ZSC).

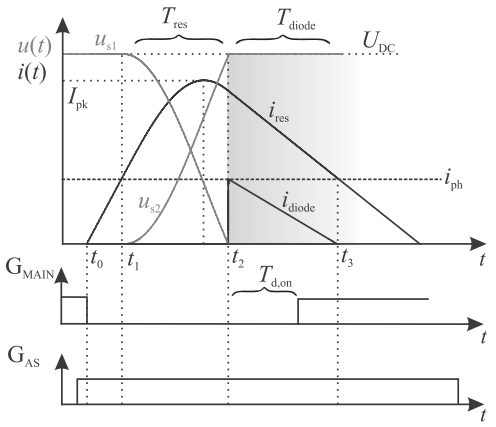

Fig. 12. Resonance caused by unsymmetrical voltage during initiating. No boost current for a successful recharging is needed. From bottom switch to top switch.

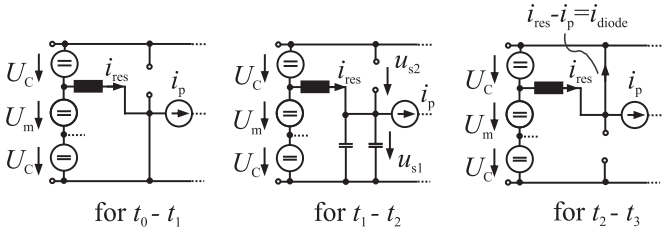

Fig. 13. Equivalent circuits for the MARC sequences.

with L_{aux} connected to the mid-point voltage $U_{DC}/2$, the voltage would swing up to U_{DC}. Initiating the resonance with a voltage higher than $U_{DC}/2$ would result in a resonance oscillating above the dc-link voltage. To achieve this, a second separated dc-link with three capacitors connected in series, C_{c1}, C_m, and C_{c2}, is applied instead or in parallel to the regular dc-link capacitors. Instead of initiating the resonance with $U_{DC}/2$ as it is done on the classic ARCP [8], the initial voltage can be set higher by selecting the ratio between the three capacitors. Thus, the mid-point capacitor C_m supports both commutations—from bottom to top and top to bottom. Example of a commutation from the bottom to the top is illustrated in Fig. 12.

To derive the equations of the MARC commutations, three equivalent circuits representing the sequences are given in Fig. 13. Here, the voltages of the capacitors $U_{C1} = U_{C2} = U_C$ are equal resulting in an initial voltage of $U_C + U_m > U_{DC}/2$. When the oscillation reaches the dc-link voltage, the anti-parallel diode starts to conduct and the residual energy of the resonant tank is fed back into the dc-link, creating a zero-voltage condition at the main switch, as shown in Fig. 12. The auxiliary inductor L_{aux} will then be demagnetized. The slope di_{res}/dt and thus the demagnetization time can be chosen by selecting U_m accordingly. For simplicity, the phase current i_p during the commutation is assumed to be constant. However, the diode conduction time is reduced whenever an inductive element is connected. The resonant current i_{res}(t) of the MARC concept is given in (14).

$$i_{res}(t) = \begin{cases} \frac{U_{DC}(1+r_m)}{2L_{aux}} t & t_0 \le t < t_1 \\ i_p + \frac{U_{DC}(1+r_m)}{2Z_{aux}} \sin(w_{aux}(t-t_1)) & t_1 \le t < t_2 \\ i_{res}(t_2) - \frac{U_{DC}(1-r_m)}{2L_{aux}}(t-t_2) & t_2 \le t < t_3 \end{cases} \tag{14}$$

with $Z_{aux} = \sqrt{\frac{L_{aux}}{2C_{sn}}}, w_{aux} = \frac{1}{\sqrt{2L_{aux}C_{sn}}}, r_m = \frac{U_m}{U_{DC}}$.

The peak current can be described by (15).

$$I_{\mathrm{pk}} = i_{\mathrm{p}} + \frac{U_{\mathrm{DC}}(1+r_{\mathrm{m}})}{2Z_{\mathrm{aux}}}. \tag{15}$$

Without additional phase current, the voltage u_{s1} is described by (16).

$$u_{\mathrm{s1}}(t) = U_{\mathrm{DC}}\left(1+\left(\frac{1+r_{\mathrm{m}}}{2}\cos\left(w_{\mathrm{aux}}(t-t_1)\right)-1\right)\right) \quad \text{for } t_1 \le t < t_2. \tag{16}$$

As previously explained, the turn-on time $T_{\mathrm{d,on}}$ is of crucial importance for the converter's safe operation. In the modified concept, the voltage of the capacitor U_{m} has direct impact on the diode conduction time T_{Diode} and, thus, $T_{\mathrm{d,on}}$ can be compensated. The diode conduction time T_{Diode} can be derived analytically as given in (17). Equation (17) is valid when the converter would operate in hard switching without activated MARC.

$$T_{\mathrm{Diode}} = \frac{2}{1-r_{\mathrm{m}}}\sqrt{\frac{2r_{\mathrm{m}}}{w_{\mathrm{res}}^2}}. \tag{17}$$

This means that the diode conduction time caused by the phase current i_{p} of the present operation state does not exceed the diode conduction time caused by the resonant tank.

Whenever the amount of the phase current i_{p} is too small to overcome the delays, the auxiliary switches must be triggered to support (in case of phase current of proper direction) or even to force (in case of phase current counteracting) the commutation.

By solving (17) to the ratio of the middle capacitor r_{m}, the delay times $T_{\mathrm{d,on}}$ of the system can be taken into account, resulting in (18).

$$r_{\mathrm{m}} \ge 1 + \frac{2}{(w_{\mathrm{aux}}T_{\mathrm{d,on}})^2}\left(1-\sqrt{(T_{\mathrm{d,on}}w_{\mathrm{res}})^2+1}\right). \tag{18}$$

In the simplified approach and for the given setup with the component values given in Table I, the commutation process should commutate with a voltage $U_{\mathrm{m}} \ge 1050$ V, e.g., $r_{\mathrm{m}} = 0.21$.

As indicated, (17) and (18) are valid when the output phase current i_{p} is constant, i.e., when the output inductance is much larger than the resonant inductance L_{aux}. Whenever the DAB transformer has small leakage inductance values compared to those of the auxiliary inductors, the diode conduction time is reduced, regardless of the current direction. In the equivalent circuit given in Fig. 13, the current source must be replaced by L_σ and differential equations of third order must be considered. For positive phase currents within the sequence $t_0 \le t < t_1$, the same equations hold true. In this sequence, the phase current i_{p} freewheels via the anti-parallel diode, and the auxiliary inductor is magnetized by the voltage $U_{\mathrm{DC}}\frac{1+r_{\mathrm{m}}}{2}$. In the second sequence $t_1 \le t < t_2$, the differential equations given in (19) describe the resonant commutation for positive (counteracting) phase current i_{p}, representing the worst case condition.

$$\begin{aligned}\frac{\mathrm{d}i_{\mathrm{res}}}{\mathrm{d}t} &= \frac{1}{L_{\mathrm{aux}}}\left(U_{\mathrm{DC}}\frac{1+r_{\mathrm{m}}}{2}-u_{\mathrm{C,sn}}(t)\right)\\ \frac{\mathrm{d}u_{\mathrm{c,sn}}}{\mathrm{d}t} &= \frac{1}{2C_{\mathrm{sn}}}(i_{\mathrm{res}}(t)-i_{\mathrm{p}}(t))\\ \frac{\mathrm{d}i_{\mathrm{p}}}{\mathrm{d}t} &= \frac{1}{L_\sigma}u_{\mathrm{C,sn}}(t)\end{aligned} \tag{19}$$

$$\text{with } L_\sigma = \frac{3}{2}L_\sigma.$$

Hence, the snubber voltage $u_{\mathrm{C,sn}}^{\mathrm{II}}(t)$, given in (20), the resonant current $i_{\mathrm{res}}^{\mathrm{II}}(t)$, and the phase current $i_{\mathrm{p}}^{\mathrm{II}}(t)$ can be derived.

$$u_{\mathrm{C,sn}}^{\mathrm{II}}(t) = \frac{1+r_{\mathrm{m}}}{2}U_{\mathrm{DC}}\frac{L_\sigma}{L_\sigma+L_{\mathrm{aux}}}\left(\cos(w_{\mathrm{M}}t)-1\right) \quad \text{for } t_1 \le t < t_2 \text{ with } w_{\mathrm{M}} = \sqrt{\frac{L_{\mathrm{aux}}+L_\sigma}{2C_{\mathrm{sn}}L_{\mathrm{aux}}L_\sigma}}. \tag{20}$$

The commutation time $T_{\mathrm{com,II}}$ in the MARC concept can then be computed by $u_{\mathrm{C,sn}}^{\mathrm{II}}(T_{\mathrm{com,II}}) = U_{\mathrm{DC}}$ as given in (21)

$$T_{\mathrm{com,II}} = \frac{2}{w_{\mathrm{M}}}\arcsin\sqrt{\frac{L_\sigma+L_{\mathrm{aux}}}{L_\sigma(r_{\mathrm{m}}+1)}}. \tag{21}$$

The diode current $i_{\mathrm{diode}}(T_{\mathrm{com,II}})$ in the moment of commutation can be calculated by (22)

$$\begin{aligned}i_{\mathrm{diode}}^{\mathrm{II}}(T_{\mathrm{com,II}}) &= i_{\mathrm{res}}^{\mathrm{II}}(T_{\mathrm{com,II}}) - i_{\mathrm{p}}^{\mathrm{II}}(T_{\mathrm{com,II}})\\ &= U_{\mathrm{DC}}\frac{1+r_{\mathrm{m}}}{2}\frac{2C_{\mathrm{sn}}L_\sigma}{L_{\mathrm{aux}}+L_\sigma}w_{\mathrm{M}}\sin(w_{\mathrm{M}}T_{\mathrm{com,II}}).\end{aligned} \tag{22}$$

Additionally, during demagnetization for $t_2 \le t < t_3$, the initial current $i_{\mathrm{diode}}^{\mathrm{II}}(t_2)$ of the anti-parallel diode must fulfill the time criteria $T_{\mathrm{d,on}}$ and thus resulting in (23).

$$i_{\mathrm{diode}}^{\mathrm{II}}(t_2) = U_{\mathrm{DC}}T_{\mathrm{d,on}}\left(\frac{1-r_{\mathrm{m}}}{2L_{\mathrm{aux}}}+\frac{1}{L_\sigma}\right). \tag{23}$$

Subsequently, (21) and (22) should be equal for $T_{\mathrm{com,II}}$ resulting in (24) and solved for $r_{\mathrm{m}}^{\mathrm{II}}$.

$$i_{\mathrm{diode}}^{\mathrm{II}}(T_{\mathrm{com,II}}) \stackrel{!}{=} i_{\mathrm{diode}}^{\mathrm{II}}(t_2). \tag{24}$$

An analytical solution is found for $r_{\mathrm{m}}^{\mathrm{II}}$, given in (25) shown at the bottom of this page.

Additionally, (21) and 22 are plotted in Fig. 15 with the values given in Table I. The minimal required diode current can be computed to $i_{\mathrm{diode}}^{\mathrm{II}}(t_2) \approx 732$ A.

Finally, when considering the transformer inductance, the voltage ratio can be calculated to $r_{\mathrm{m}}^{\mathrm{II}} \approx 0.28$. The detailed analysis shows that r_{m} and $r_{\mathrm{m}}^{\mathrm{II}}$ differ significantly, proving the need

$$r_{\mathrm{m}}^{\mathrm{II}} = \frac{T_{\mathrm{d,on}}^2(2L_{\mathrm{aux}}^2+L_\sigma^2+3L_{\mathrm{aux}}L_\sigma)+8C_{\mathrm{sn}}^2L_{\mathrm{aux}}^2L_\sigma^2w_{\mathrm{M}}^2-4C_{\mathrm{sn}}L_{\mathrm{aux}}L_\sigma w_{\mathrm{M}}\sqrt{4C_{\mathrm{sn}}^2L_{\mathrm{aux}}^2L_\sigma^2w_{\mathrm{M}}^2+T_{\mathrm{d,on}}^2(L_{\mathrm{aux}}+L_\sigma)^2}}{T_{\mathrm{d,on}}^2L_\sigma(L_{\mathrm{aux}}+L_\sigma)} \tag{25}$$

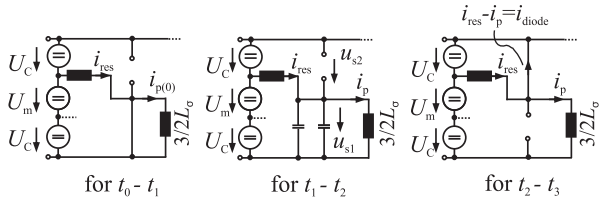

Fig. 14. Equivalent circuits for the MARC sequences for $0 < \varphi < \frac{\pi}{3}$ considering transformer leakage inductances.

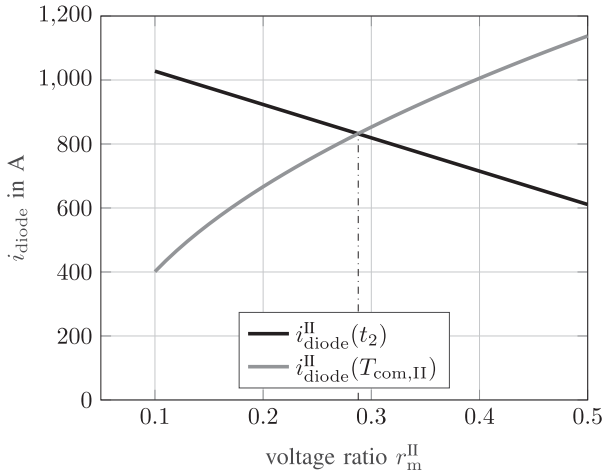

Fig. 15. Numerical solution of voltage ratio $r_{\mathrm{m}}^{\mathrm{II}}$.

for a detailed analysis. The equations for a lossless commutation have been verified using MATLAB/PLECS circuit simulation. In addition, turn-on losses, voltage drops of the semiconductor switches, and resistive losses must be considered for a precise selection of the voltage U_{m}.

To set the voltage of the middle capacitor, a galvanic isolated power supply is preferred. The power P_{Cm}, which has to be fed into the middle C_{m} capacitor, depends on the size of the snubber capacitors C_{sn}, the switching frequency f_{sw}, the amplitude of the dc-link voltage U_{DC}, and the ratio r_{m}. Considering the energy $E_{\mathrm{sn,leg}}$ of the snubber capacitors per leg, the power P_{Cm} can be estimated according to (26)

$$\begin{aligned} P_{\mathrm{Cm}} &= \frac{2r_{\mathrm{m}}}{1-r_{\mathrm{m}}} 3 f_{\mathrm{sw}} E_{\mathrm{sn,leg}} \\ &= \frac{2r_{\mathrm{m}}}{1-r_{\mathrm{m}}} 3 f_{\mathrm{sw}} C_{\mathrm{sn}} U_{\mathrm{DC}}^2 \\ &\approx 57\,\mathrm{kW}. \end{aligned} \tag{26}$$

With the data given in Table I and $r_{\mathrm{m}}^{\mathrm{II}} = 0.28$, an average power of $P_{\mathrm{Cm}} = 57$ kW at a rms current of ≈35 A is required. Here, an auxiliary winding added to the existing transformer is proposed, which can be set to the required ratio $r_{\mathrm{m}}^{\mathrm{II}}$. Thus, the voltage ratio is always constant, and variations in the dc-link voltage do not affect the system. Since the circulated power is not of a high amount and the core of the medium-frequency transformer already exists, only additional windings and a simple diode rectifier are required.

In Fig. 16, an exemplary transformer configuration, with the auxiliary windings highlighted in gray, is presented.

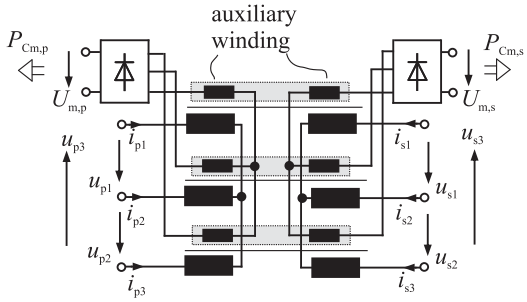

Fig. 16. Medium-frequency transformer with auxiliary windings to ensure constant voltage of the middle capacitors.

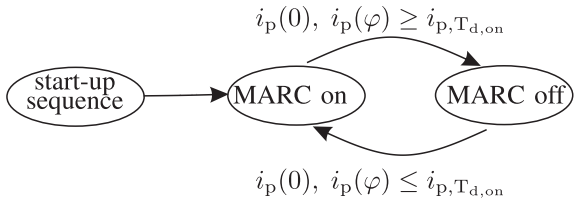

Fig. 17. Operation strategy of the converter.

Using a three-phase diode rectifier allows to shrink the size of C_{m}. The characteristic 50% duty cycle of the DAB and the three-phase system guarantees constant input voltage from the ac link.

The MARC concept is a self-balancing topology regarding the dc-link capacitor. The voltage of the middle capacitor is always fixed due to the ratio of the auxiliary windings. In case the voltage is $U_{\mathrm{C1}} < U_{\mathrm{C2}}$, the resonance from bottom to top is generated with $U_{\mathrm{C1}} + U_{\mathrm{m}}$. Due to the higher voltage, the resonant current will be higher as well and the additional energy will be fed back into the upper capacitor C_2, which will then rise in voltage. On the other hand, the resonance from bottom to top causes a lower peak current, and less energy is circulated back to the lower capacitor.

V. Operation Strategy of the Converter

The basic operation is initiated with the start-up sequence described in [33] and briefly described in the following. Since the converter is supposed to be installed into a dc-grid where voltage can be supplied before switching, the converter must be capable of a black start. The main switches are protected using the ZVD and cannot be turned on if a voltage across a switch is higher than 25 V. Here, the bottom snubber capacitors of the primary and secondary converters are first discharged using the zero-state chopper (ZSC), shown in Fig. 11, which consists of a switch, a series diode, and a resistor. Thus, the converter can be started from a defined switching state. Here, the converter is started to operate, beginning with all bottom switches turned on.

Since the switch of the ZSC is selected only for discharging of the snubber capacitors at low power, a current into its anti-parallel diode must be avoided. Thus, a series diode is needed to ensure that a positive phase current i_{p} commutates into the anti-parallel diodes of the main devices in the PEBB stacks.

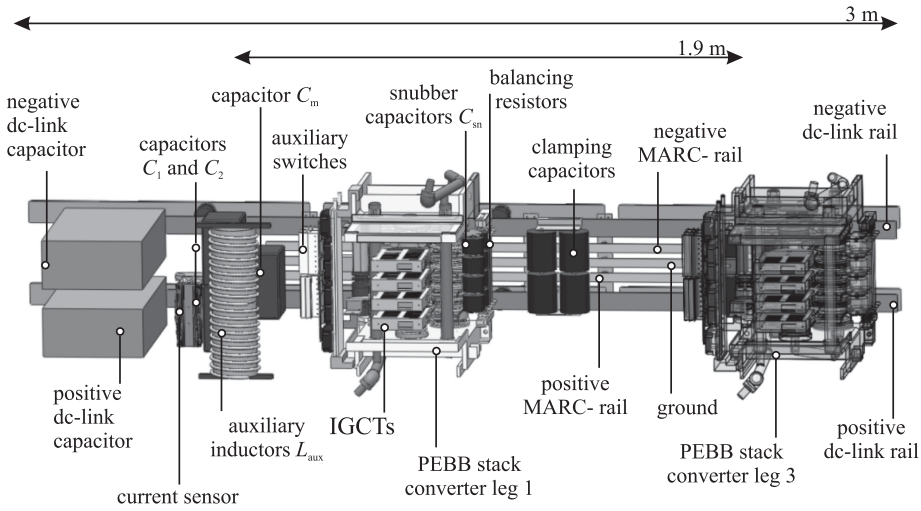

Fig. 18. Simplified CAD drawing of primary-side converter and dc-link design. For improved visibility, the second converter leg is not shown.

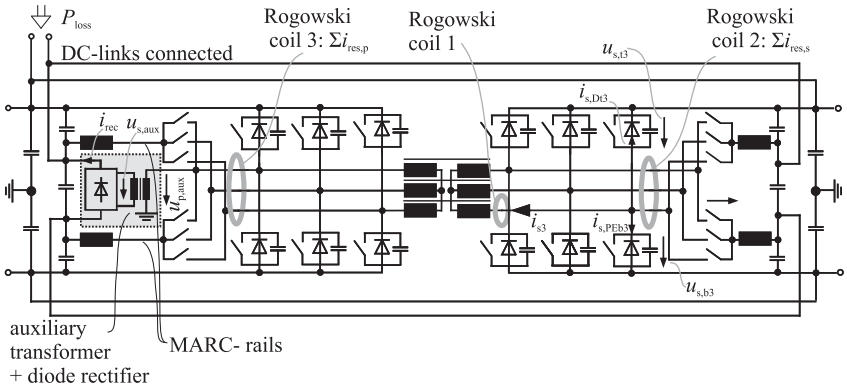

Fig. 19. Complete circuit of the test setup. Primary and secondary dc links are connected and tests are performed at a dynamic voltage ratio of $d = 1$. The capacitor C_{m} is charged by a diode rectifier and an additional auxiliary transformer which can be integrated into the existing transformer to save one additional core.

After the start-up phase, the DAB is operating in soft-switching mode supported by the MARC extension. Whenever the converter is running in natural soft-switching, the phase current $i_{\mathrm{p}}(0), i_{\mathrm{p}}(\varphi) \geq i_{\mathrm{p,T_{d,on}}}$ and the auxiliary switches can be left off. Thus, conduction losses of the inductor and switches are saved and the efficiency increases. If the phase current decreases again, the DAB must be supported by the quasi-resonant switching again; otherwise, the converter will stop its operation. The flowchart of the operation strategy is illustrated in Fig. 17.

This is different to conventional clamping circuits for IGCTs, since the losses due to the diode clamping will increase with higher load currents. For the presented high-power setup in [24], a simulative approach prospects loss savings of 50 kW in partial load under ARCP operation at 2 MW, but also 50 kW in high-power operation at 5 MW when the ARCP is left off.

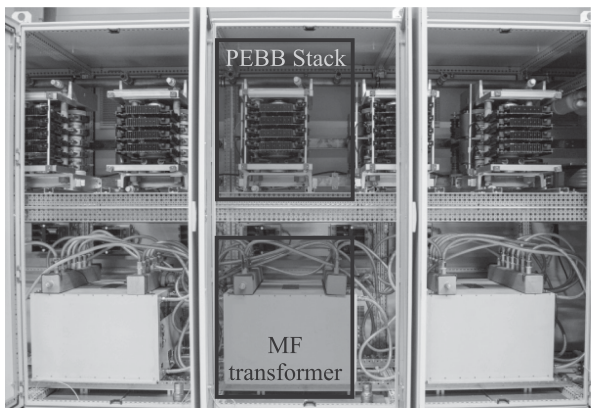

Fig. 20. General setup used for measurements: highlighted the medium-frequency (MF) transformers and the PEBB stacks.

VI. Experimental Setup

All components of the modified setup are fully integrated in the cabinets as illustrated in Fig. 20. The electronics are located at the top of the cabinets and the three single-phase transformers (600 kg per transformer) at the bottom. A 3D CAD presentation of the primary converter is given in Fig. 18. Here, the general arrangement of the PEBB stacks, the copper rails, the

TABLE II
SYSTEM COMPONENTS

Component	Value	Manufacturer	Reference
Main active switch	5SHY35L4510	ABB	[38]
Free-wheeling diode	D1031SH	Infineon	[37]
Capacitors $C_{\mathrm{dc},1}$, ...	2 mF, 3200V	FPX	
Capacitors C_1, C_2, C_m	200µF, 2800V	FPX	
Auxiliary inductor	12 µH	self-produced	
Auxiliary IGBT	FZ800R45KL3	Infineon	[41]
ARCP SiC diodes	IDW40G120C5B	Infineon	[40]

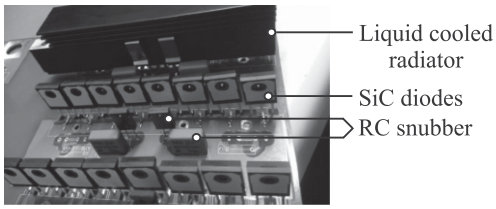

Fig. 21. SiC diodes soldered on a printed circuit board to suppress reverse recovery. Three diodes connected in series and eight in parallel.

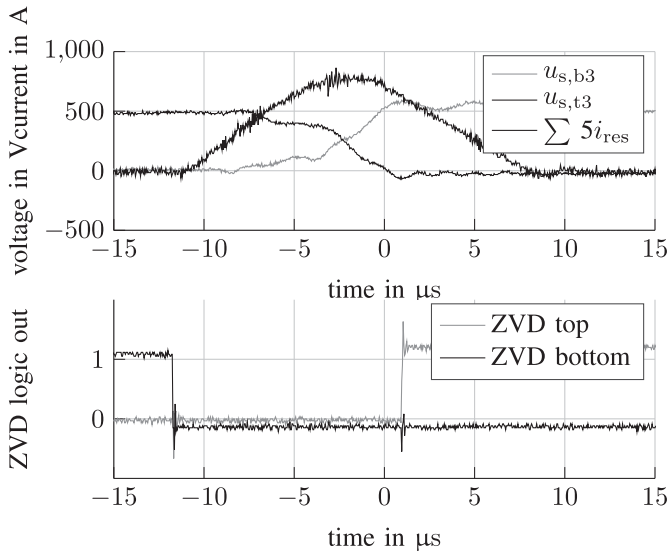

Fig. 22. Commutation phase of a modified PEBB stack including the ZVD logic signals.

auxiliary devices, and passive components is given. The auxiliary switches (AS) and snubber capacitors C_sn are mounted as close as possible to the IGCT PEBB stacks [36]. The separated dc-link for the MARC is in parallel to the classic dc-link as shown. The auxiliary inductors L_aux are mounted close to the separated dc link. They are connected to the MARC copper rails to which all PEBB stacks are connected as well. Due to the distance to the capacitors $C_{\mathrm{dc},1}$, $C_{\mathrm{dc},2}$, and C_m, the resulting auxiliary inductance increases for the second and third stacks, as shown in the test results.

The primary converter has a length of 3 m. The complete DAB is about 7 m long, including water pumps and deionization units. Water-to-air heat exchangers are mounted on the roof of the laboratory.

In Table II, the key components of the converter are summarized.

One auxiliary switch for one PEBB stack is constructed using two Infineon FZ800R45KL3 medium-voltage IGBTs connected in series with 3×8 1.2 kV SiC diodes as shown in Fig. 21. Using SiC diodes almost eliminates the reverse recovery. The circuit of the experimental setup is given in Fig. 19.

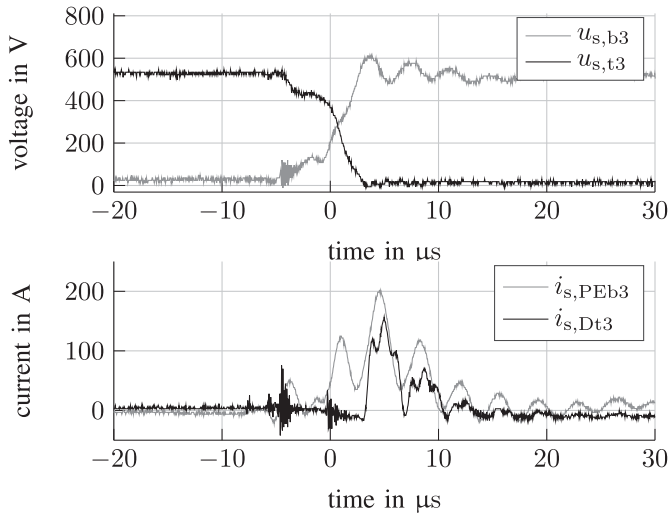

Fig. 23. Detailed commutation phase, and high oscillations during current commutation with fast diodes.

VII. EXPERIMENTAL RESULTS

In the following, initial test results conducted with the experimental setup up to a dc-link voltage of 500 V are presented. The dc links of the primary and secondary sides are connected to each other; only the power losses of the converters need to be supplied by an external power supply.

In Fig. 22, one commutation of leg s3 (according to Fig. 1) and the voltages $u_{\mathrm{s,t3}}$, $u_{\mathrm{s,b3}}$ and the resonant current is plotted. Overshoots of 20% and the a peak resonant current of 75 A are measured. The gate signals of the ZVD are additionally measured to show the turn on and turn off of each PEBB stack.

Fig. 23 plots the current distribution within the PEBB stack s3. Although the capacitor voltages and the resonant current show almost ideal behavior, high current oscillation in the PEBB stacks accrues. Since high-power devices have high space charges, and thus capacitance, high oscillations occur during commutation. Very fast diodes were added temporarily to illustrate the commutation from the resonant capacitors into the anti-parallel diode.

As derived analytically, the ratio r_m has a direct impact on the diode conduction time. For illustration, various ratios r_m were applied by changing the winding configurations of the auxiliary transformer. The results are plotted in Fig. 24.

As mentioned, the start-up sequence is needed whenever the dc-link and thus the resonant capacitors are pre-charged. To overcome the floating state of the converter, the zero-state choppers are turned on. In Fig. 25, the start-up sequence is plotted.

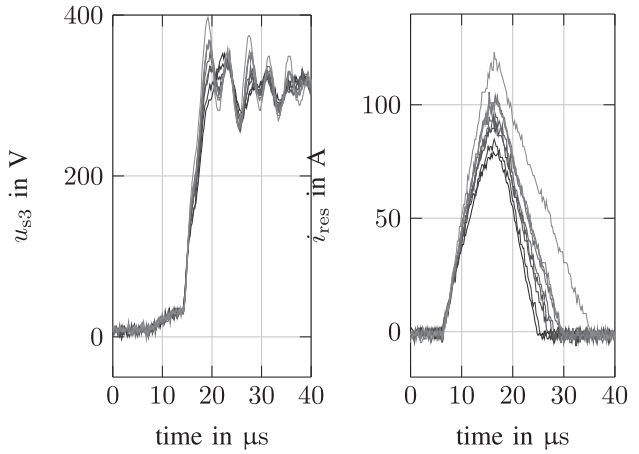

Fig. 24. Resonant phase and diode conduction time manipulated with various $r_m = 0.1$–0.7 illustrating the impact at a dc-link voltage of 300 V.

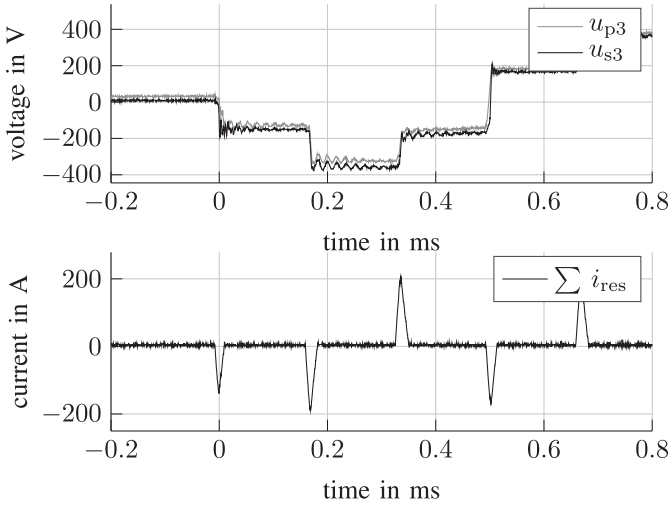

Fig. 25. Start-up phase of the three-phase system initiated with the zero-state choppers.

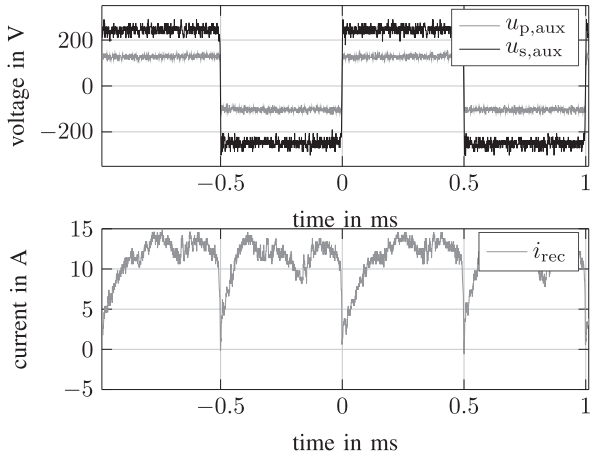

Fig. 26. Input and output voltage of the auxiliary transformer $u_{p,aux}$, $u_{s,aux}$ and the rectifier output current i_{rec}. Transformer supplies both middle capacitors.

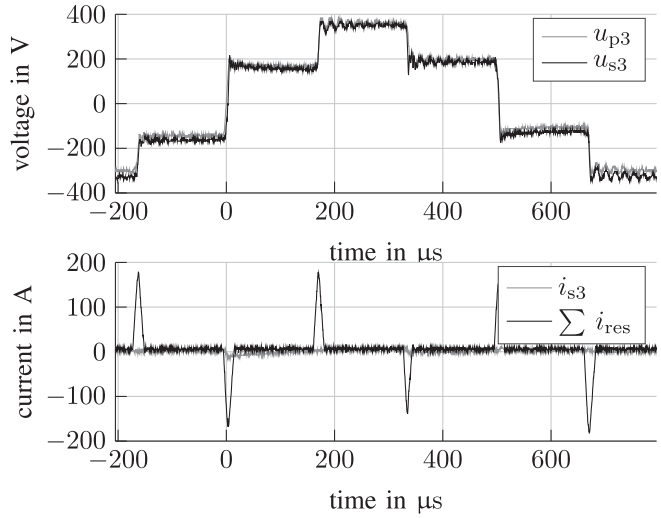

Fig. 27. No-load operation of the three-phase DAB.

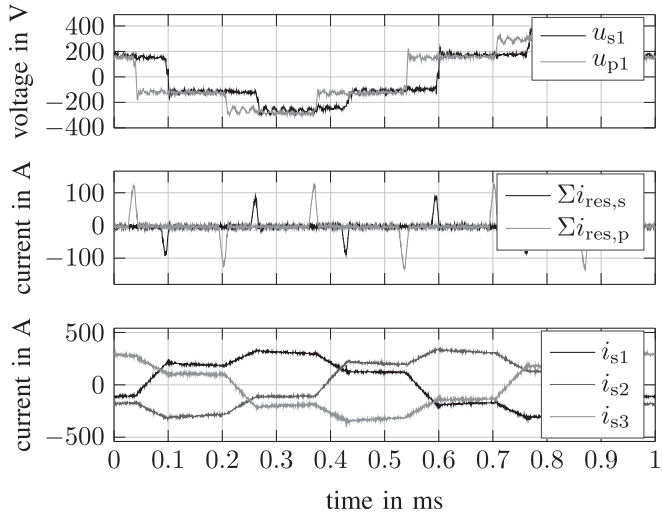

Fig. 28. Operation under phase-shift of the three-phase system. The peak-resonant currents decrease due to supporting load current.

The primary and secondary voltages of the auxiliary transformer and the output current of the diode-rectifier i_{rec} are plotted in Fig. 26.

Fig. 27 shows the plot of a dc-link voltage of 400 V at zero-phase shift $\varphi = 0$. The characteristic six-step voltage of the primary and secondary sides in the DAB are visible and the phase current i_p is negligible. Due to the large setup, the peak resonant currents of each converter leg change depending on its distance to the resonant inductor and the dc-link, hence L_{aux} increases with greater distance.

In Fig. 28, the results are plotted at a higher phase shift with a phase current of up to $i_p = 380$ A. The inductive load currents support the commutations in time and damps the resonance. Thus, the peak resonant currents on the primary and secondary sides decrease.

VIII. Conclusion and Outlook

Whenever a dual-active bridge converter is equipped with lossless snubber capacitors, the soft-switching area is reduced. The snubber size has a strong impact on the soft-switching range, as was analytically derived. The presented prototype is constructed with IGCT power electronic modules with integrated gate drivers. It was shown that these power modules have long turn-on delay times, which limit the soft-switching area further. To overcome these challenges, the ARCP concept was introduced. However, precise control of the required boost current was found to be a major challenge with the existing gate drivers. To overcome these issues, a novel auxiliary circuit that does not require boost current control was introduced to commutate the snubber capacitors, which are placed in parallel to the main IGCTs. This modified ARCP circuit, simply called MARC, uses a mid-point capacitor to set off the voltage that drives the auxiliary resonant current above the dc-link mid-point voltage. Consequently, the commutation of the snubber capacitors does not require any boost current. Hence, no additional fast boost current control is needed, as is necessary for the classical ARCP concept. This leads to a reduced control complexity and cost reduction. Losses and delays can be compensated easily by choosing the voltage of the mid-point capacitor U_{m} properly. The presented setup uses auxiliary switches constructed with medium-voltage IGBTs in combination with SiC diodes to suppress the reverse recovery losses of the converter. This contributes to achieve higher efficiencies. The resonant inductor is rated for the resonant rms current, which is much lower in contrast to the $\frac{\mathrm{d}i}{\mathrm{d}t}$limiter that is needed in hard-switched IGCT-based converter systems carrying the complete dc-link current.

PROS

1) higher efficiency
2) no clamping circuit needed
3) simple control
4) reduced EMI
5) limited $\frac{\mathrm{d}u}{\mathrm{d}t}$
6) self-balancing dc-link
7) no complex boost current control

CONS

1) higher amount of devices
2) slightly higher investment

The MARC concept requires an additional galvanic isolated power source for constant voltage of the mid-point capacitor. It is shown that this auxiliary power supply can be powered by the main switches. Its auxiliary transformer can be integrated in the DAB transformers by adding windings into the DAB medium-frequency transformers, both at the primary and secondary sides.

Acknowledgment

The authors would like to thank Infineon Technology AG and ABB for donating various components.

References

[1] A. Riccobono *et al.*, "Next generation automation architecture for DC smart homes," in *Proc. IEEE Int. Energy Conf. (ENERGYCON)*, Leuven, Belgium, 4–8 Apr., 2016, pp. 1–6.

[2] R. W. D. Doncker, "Power electronic technologies for flexible DC distribution grids," in *Proc. Int. Power Electron. Conf., IPEC-Hiroshima ECCE-ASIA*. E.ON ERC at RWTH Aachen University, Institute for Power Generation and Storage Systems, 2014, pp. 736–743.

[3] R. W. De Doncker, D. M. Divan, and M. H. Kheraluwala, "A three-phase soft-switched high-power-density DC/DC converter for high-power applications," *IEEE Trans. Ind. Appl.*, vol. 27, no. 1, pp. 63–73, Jan./Feb. 1991.

[4] R. W. D. Doncker, D. M. Divan, and M. H. Kheraluwala, "Power conversion apparatus for DC/DC conversion using dual active bridges," U.S. Patent 5 027 264A, Sep. 29, 1989/Jun. 1991.

[5] F. Krismer and J. W. Kolar, "Efficiency-optimized high current dual active bridge converter for automotive applications," *IEEE Trans. Ind. Elect.*, vo1. 59, no. 7, pp. 2745–2760, Jul. 2012.

[6] M. Kheraluwala, R. Gascoigne, D. Divan, and E. Baumann, "Performance characterization of a high-power dual-active bridge dc-to-dc converter," *IEEE Trans. Ind. Appl.*, vol. 28, no. 6, pp. 1294–1301, Nov. 1992.

[7] R. Lenke, "A contribution to the design of isolated DC–DC converters for utility applications," Ph.D. dissertation, RWTH Aachen Univ., 2010.

[8] R. W. D. Doncker and J. P. Lyons, "The auxiliary resonant commutated pole converter," in *Proc. Industry Appl. Soc. Annu. Meeting*, 1990, pp. 1225–1231.

[9] W. Dong, J.-Y. Choi, F. C. Lee, D. Boroyevich, and J. Lai, "Comprehensive evaluation of auxiliary resonant commutated pole inverter for electric vehicle applications," in *Proc. IEEE 32nd Annu. Power Electron. Specialists Conf.* (IEEE Cat. No. 01CH37230), 2001, pp. 625–630.

[10] R. Teichmann, "Control parameter selection in auxiliary resonant commutated pole converters," in *Proc. 27th Annu. Conf. IEEE Industrial Electron. Society*, IECON, 2001, pp. 862–869.

[11] S. Bernet, R. Teichmann, J. Weber, and P. K. Steimer, "Evaluation of a high power ARCP voltage source inverter with IGCT," in *Proc. Industry Applications Conf.*, *34th IAS Annual Meeting*. Conference Record of the 1999 IEEE, pp. 1063–1072.

[12] W. Yue, L. Ning, Z. Changsong, C. Wulong, L. Wanjun, and Wang Zhao, "A clamping circuit parameter design method for IGCT used in high power applications," in *Proc. IEEE Appl. Power Electron. Conf. Expo. – APEC*, Fort Worth, TX, USA, 24 Apr. 2014, pp. 3406–3410.

[13] M. D. Bellar, T.-S. Wu, A. Tchamdjou, J. Mahdavi, and M. Ehsani, "A review of soft-switched DC–AC converters," *IEEE Trans. Ind. Appl.*, vol. 34, no. 4, pp. 847–860, Jul./Aug. 1998.

[14] A. Toba, T. Shimizu, G. Kimura, M. Shioya, and S. Sano, "Auxiliary resonant commutated pole inverter using two internal voltage-points of DC source," *IEEE Trans. Ind. Electron.*, vol. 45, no. 2, pp. 200–206, Apr. 1998.

[15] J. G. Cho, J. W. Baek, D. W. Yoo, C. Y. Won, and G. H. Rim, "Zero-voltage-switching three-level auxiliary resonant commutated pole inverter for high-power applications," in *IEEE Proc. Elect. Power Appl.*, vol. 145, no. 1, pp. 25–32, Jan. 1998, doi: 10.1049/ip-epa:19981421.

[16] F. R. Dijkhuizen and J. L. Duane, "Basic auxiliary resonant pole (ARP) applied to three-level nested cells switching leg," in *Proc. 35th Annu. IEEE Power Electron. Specialists Conf.*, Aachen, Germany, 2004, pp. 4434–4440.

[17] Z. Y. Pan and F. L. Luo, "Novel resonant pole inverter for brushless DC motor drive system," *IEEE Trans. Power Electron.*, vol. 20, no. 1, pp. 173–181, Jan. 2005.

[18] J. Shukla and B. G. Fernandes, "Quasi-resonant dc-link soft-switching PWM inverter with active feedback clamp circuit for motor drive applications," *IEEE Proc. Elect. Power Appl.*, vol. 153, no. 1, pp. 75–82, Jan. 2006.

[19] E. Chu, M. Wu, L. Huang, X. Hou, and H. Zhang, "Research on a novel modulation strategy for auxiliary resonant commutated pole inverter with the smallest loss in auxiliary commutation circuits," *IEEE Trans. Power Electron.*, vol. 29, no. 3, pp. 1103–1117, Mar. 2014.

[20] A. Safaee, P. Jain, and A. Bakhshai, "A ZVS pulsewidth modulation full-bridge converter with a low-RMS-current resonant auxiliary circuit," *IEEE Trans. Power Elec.*, vol. 31, no. 6, Jun. 2016.

[21] K. Ali, P. Das, and S. K. Panda, "Analysis and design of APWM half-bridge series resonant converter with magnetizing current assisted ZVS," *IEEE Trans. Ind. Elec.*, vol. 64, no. 3, Mar. 2017.

[22] Y. Chen, A. S. Sathyanarayanan, B. Narayanasamy, W. Feng, and F. Luo, "Comprehensive evaluation of interleaved zero current switching inverter against interleaved hard switching inverters in terms of efficiency, power density and EMI spectrum," in *Proc. IEEE Appl. Power Electron. Conf. Expo. (APEC)*, Tampa, FL, USA, School of Electrical and Computer Engineering, The Ohio State University 2017.
[23] A. Charalambous, X. Yuan, and N. McNeill, "High-frequency EMI attenuation at source with the auxiliary commutated pole inverter," *IEEE Trans. Power Electron.*, vol. 33, no. 7, pp. 5660–5676, Jul. 2018.
[24] J. Voss, B. Bagaber, and R. W. De Doncker, "Full soft-switching capability of the dual-active bridge by using the auxiliary-resonant commutated-pole technique," in *Proc. IEEE 8th Int. Symp. Power Electron. Distributed Generation Syst., PEDG*, Florianopolis, Brazil, Apr. 2017, pp. 1–8.
[25] J. Hu, Z. Yang, N. Soltau, and R. W. D. Doncker, "A duty-cycle control method to ensure soft-switching operation of a high-power three-phase dual-active bridge converter," in *Proc. IEEE 3rd Int. Future Energy Electron. Conf. ECCE Asia*, 2017, pp. 866–871.
[26] G. Kimura, T. Shimizu, A. Toba, and S. Sano, "Quasi-resonant PWM inverter," Yuasa Corporation, U.S. Patent 5 572 418, Osaka Prefecture, Japan, Sep. 1993.
[27] A. Toba, T. Shimizu, G. Kimura, M. Shioya, and S. Sano, "Auxiliary resonant commutated pole inverter using two internal voltage-points of DC source," *IEEE Trans. Ind. Electron.*, vol. 45, no. 2, pp. 200–206, Apr. 1998.
[28] R. W. De Doncker, D. M. Divan, and M. H. Kheraluwala, "A three-phase soft-switched high-power-density DC/DC converter for high-power applications," *IEEE Trans. Ind. Appl.*, vol. 27, no. 1, pp. 63–73, Jan./Feb. 1991, doi: 10.1109/28.67533.
[29] N. H. Baars, J. Everts, C. G. E. Wijnands, and E. A. Lomonova, "Evaluation of a high-power three-phase dual active bridge DC–DC converter with three-level phase-legs," in *Proc. 18th Eur. Conf. Power Electron. Appl. (EPE'16 ECCE Europe)*, Karlsruhe, 2016, pp. 1–10, doi: 10.1109/EPE.2016.7695616.
[30] H. V. Hoek, "Design and operation considerations of three-phase dual active bridge converters for low-power applications with wide voltage ranges," Ph.D. dissertation, RWTH Aachen Univ., Aachen, 2016, ISBN 978-3-8440-5011-0, 2017.
[31] S. Karys, "Selection of resonant circuit elements for the ARCP inverter," in *Proc. 10th Int. Conf. Elect. Power Quality Utilization*, 2009, pp. 1–6.
[32] K. Ma, D. Xu, T. Zhang, and S. Igarashi, "The evaluation of control strategies for auxiliary resonant commutated pole inverter," in *Proc. IEEE Energy Conversion Congress Expo.*, 2009, pp. 810–816.
[33] J. Voss, J. Henn, and R. W. D. Doncker, "Control techniques of the auxiliary-resonant commutated pole in the dual-active bridge," in *Proc. 12th IEEE Int. Conf. Power Electron. Drive Syst.*, 2017, Honolulu, HI, USA, Dec. 12–15, 2017, pp. 972–978.
[34] P. Koellensperger, J. V. Bloh, S. Schroeder, and R. W. De Doncker, "A GCT-driver optimized for soft-switching high-power inverters with short circuit protection," in *Proc. 35th Annu. IEEE Power Electron. Specialists Conf.*, 2004, pp. 105–111.
[35] ABB, *APPLICATION NOTE 5SYA 2031-05. Applying IGCT Gate Units*. Lenzburg, Switzerland: ABB Switzerland Ltd. Semiconductors.
[36] ABB, *ACS 6000 Medium Voltage Drives – Service and Maintenance Manual*. Lenzburg, Switzerland: ABB Switzerland Ltd., 2005.
[37] ABB Switzerland Ltd. Semiconductors, *Fast Recovery Diode 5SDF 13H4501*. Lenzburg, Switzerland: ABB Switzerland Ltd., 2006. Available: http://www.5scomponents.com/pdf/5SDF13H4501.pdf
[38] ABB Switzerland Ltd. Semiconductors, *Application Note: Applying IGCTs*. Lenzburg, Switzerland: ABB Switzerland Ltd., 2016. Available: https://library.e.abb.com/public/
[39] Infineon Technology AG, *D1031SH*. Datasheet. Infineon Technology AG. [Online]: Available: http://www.infineon.com/dgdl/Infineon-D1031SH-v8_1_en-de.pdf
[40] ABB Switzerland Ltd. Semiconductors, *Application Note: Applying IGCTs*. Lenzburg, Switzerland: ABB Switzerland Ltd., 2014. Available: https://library.e.abb.com/public/
[41] AVX, *Datasheet FPX86*. AVX, 2006. Available: http://datasheets.avx.com/fpx.pdf
[42] Infineon Technology AG, *Silicon Carbide Schottky Diode, IDW40G120C5B*. Datasheet. Infineon Technology AG, 2017. [Online]. Available: https://www.infineon.com/dgdl/Infineon-IDW40G120C5B-DS-v02_01-EN.pdf
[43] Infineon Technology AG, *FZ800R45KL3_B5 High Insulated Module With Trench/Fieldstop IGBT3 and Emitter Controlled Diode*. Datasheet. Infineon Technology AG, 2018. [Online]. Available: https://www.infineon.com/dgdl/Infineon-FZ800R45KL3_B5-DS-v03_02-EN.pdf

Johannes Voss received the Diploma degree in electrical engineering from RWTH Aachen University, Aachen, Germany, in 2011.

He joined the Institute for Power Generation and Storage Systems (PGS), E.ON Energy Research Center, RWTH Aachen University. In 2015, he was with the NSF GRid-connected Advanced Power Electronics Systems (GRAPES) at the University of Arkansas as an Exchange Student, for a period of eight months, under the lead of Prof. Dr. Mantooth. His research interests include the field of power electronics.

Rik W. De Doncker (F'01) received the Ph.D. degree in electrical engineering from the Katholieke Universiteit Leuven, Leuven, Belgium, in 1986.

In 1987, he was a Visiting Associate Professor with the University of Wisconsin, Madison, WI, USA. In 1989, he joined the Corporate Research and Development Center, General Electric Company, Schenectady, NY, USA. In 1994, he joined Silicon Power Corporation, a former division of General Electric Inc., as the Vice President of Technology. In 1996, he was a Professor with RWTH Aachen University, Aachen, Germany, where he currently leads the Institute for Power Electronics and Electrical Drives. Since 2006, he has been the Director of the E.ON Energy Research Center, RWTH Aachen University.

Dr. De Doncker was the President of the IEEE Power Electronics Society (PELS) in 2005 and 2006. He was the Founding Chairman of the German IEEE Industry Applications Society PELS Joint Chapter. In 2002, he was the recipient of the IEEE IAS Outstanding Achievement Award. In 2008, he received the IEEE PES Nari Hingorani Custom Power Award. In 2009, he led a VDE/ETG Task Force on Electric Vehicles. In 2010, he received an Honorary Ph.D. from TU Riga, Latvia. In 2013, he received the IEEE William E. Newell Power Electronics Award.